LIMNOLOGY and OCEANOGRAPHY

ASLO

Limnol. Oceanogr. 9999, 2022, 1–19

doi: 10.1002/lno.12217

Cold-water coral ecosystems under future ocean change: Live coral performance vs. framework dissolution and bioerosion

Janina Vanessa Büscher,[1*] **Armin Uwe Form**,[1] **Max Wisshak**,[2] **Rainer Kiko**,[3,4] **Ulf Riebesell**[1]

[1]GEOMAR Helmholtz Centre for Ocean Research Kiel, Research Division 2: Marine Biogeochemistry—Biological Oceanography, Kiel, Germany
[2]SENCKENBERG am Meer, Marine Research Department, Wilhelmshaven, Germany
[3]GEOMAR Helmholtz Centre for Ocean Research Kiel, Research Division 3: Marine Ecology, Kiel, Germany
[4]Laboratoire d'Océanographie de Villefranche-sur-Mer, Villefranche-sur-Mer, France

Abstract

Physiological sensitivity of cold-water corals to ocean change is far less understood than of tropical corals and very little is known about the impacts of ocean acidification and warming on degradative processes of dead coral framework. In a 13-month laboratory experiment, we examined the interactive effects of gradually increasing temperature and pCO_2 levels on survival, growth, and respiration of two prominent color morphotypes (colormorphs) of the framework-forming cold-water coral *Lophelia pertusa*, as well as bioerosion and dissolution of dead framework. Calcification rates tended to increase with warming, showing temperature optima at ~ 14°C (white colormorph) and 10–12°C (orange colormorph) and decreased with increasing pCO_2. Net dissolution occurred at aragonite undersaturation ($\Omega_{Ar} < 1$) at ~ 1000 μatm pCO_2. Under combined warming and acidification, the negative effects of acidification on growth were initially mitigated, but at ~ 1600 μatm dissolution prevailed. Respiration rates increased with warming, more strongly in orange corals, while acidification slightly suppressed respiration. Calcification and respiration rates as well as polyp mortality were consistently higher in orange corals. Mortality increased considerably at 14–15°C in both colormorphs. Bioerosion/dissolution of dead framework was not affected by warming alone but was significantly enhanced by acidification. While live corals may cope with intermediate levels of elevated pCO_2 and temperature, long-term impacts beyond levels projected for the end of this century will likely lead to skeletal dissolution and increased mortality. Our findings further suggest that acidification causes accelerated degradation of dead framework even at aragonite saturated conditions, which will eventually compromise the structural integrity of cold-water coral reefs.

The increase in carbon dioxide (CO_2) emissions in the atmosphere since the industrial revolution has led to a decrease in carbonate ion concentrations in the oceans and a lowered seawater pH by 0.1 units, a process referred to as ocean acidification (Feely et al. 2004). The rapidity and extent of ongoing ocean acidification and the resulting global warming is unmatched in Earth's history (Siegenthaler et al. 2005), with up to 0.3 units decrease in global surface ocean pH projected for the end of the century (IPCC Special Report; Bindoff et al. 2019). Lower carbonate ion concentrations result in a diminished calcium carbonate ($CaCO_3$) saturation, affecting organisms that build skeletons and shells composed of the most common marine $CaCO_3$ polymorphs, aragonite and calcite (Orr et al. 2005). In scleractinian corals, the key calcifiers in global coral reef ecosystems, skeleton formation was shown to be impaired by acidification (Mollica et al. 2018; Hennige et al. 2020).

Increased sea surface temperature due to global warming elevated by 0.56–0.92°C in the past 100 yr, with a projected average increase of 1.6–4.3°C by 2100 (Bindoff et al. 2019).

The increase in seawater temperature and CO_2 concentration also reaches deeper water layers (Tanhua et al. 2007) with implications for deep-sea corals, since these changes are particularly evident in colder waters and at high latitudes (Bindoff et al. 2019) such as the subpolar North Atlantic, where these corals commonly occur.

*Correspondence: janina.buescher@nuigalway.ie

Additional Supporting Information may be found in the online version of this article.

Author Contribution Statement: J.V.B., A.U.F., and M.W. contributed substantially to the study's conception and data acquisition. J.V.B., A.U.F., M.W., and R.K. contributed to the data analysis. J.V.B. drafted the manuscript with support from all co-authors.

About 90% of all known scleractinian bioherm-forming cold-water corals live in supersaturated waters with respect to aragonite (Davies and Guinotte 2011). Model simulations reveal that ~ 70% will be exposed to calcium carbonate undersaturated waters ($\Omega_{Ar} \leq 1$) by the end of the century due to ocean acidification (Guinotte et al. 2006; Zheng and Cao 2015), resulting in diminished habitat suitability.

Cold-water coral bioherms are important biodiversity hotspots, which are thought to be equally biodiverse as tropical coral reefs (Henry and Roberts 2017). The most abundant scleractinian cold-water coral is *Lophelia pertusa* (also referred to as *Desmophyllum pertusum*; Addamo et al. 2016), a cosmopolitan azooxanthellate species that builds large three-dimensional frameworks (Freiwald et al. 2004). More than 2700 species of associated fauna were recorded in *L. pertusa* habitats alone to date (Roberts and Cairns 2014). Much of the associated fauna is found in the "dead" coral framework beneath the live coral zone, accounting for approximately 70% of *L. pertusa* colonies (Vad et al. 2017) and is therefore of particular importance to the biodiversity of a reef.

The response of *L. pertusa* to elevated CO_2 concentrations and temperatures has been examined in several laboratory studies to assess its resilience to future climate conditions. Results indicate a potential for acclimatization to future acidified conditions with regard to calcification (Form and Riebesell 2012; Hennige et al. 2015; Büscher et al. 2017). However, although positive net growth was sustained in most experiments, calcification rates of *L. pertusa* decreased under elevated pCO_2 conditions in the majority of studies. Warming resulted in increased net calcification in a previous laboratory experiment, whereas combined acidification and warming resulted in balanced net growth with rates comparable to the control treatment kept at ambient seawater conditions (Büscher et al. 2017). This suggests that the negative effects of acidification on calcification can partially be mitigated by warming when both temperature and pCO_2 are elevated simultaneously. Such compensatory effects may, however, require additional energy or lead to depression of other physiological processes as observed in the tropical scleractinian *Pocillopora damicornis* (Jiang et al. 2018). Despite the general perception that increased energetic demands can be met by increased feeding rates as observed in some tropical corals (Holocomb et al. 2010; Edmunds 2011), recent studies have shown that not all corals can utilize additional food to compensate for extra energy demands under elevated pCO_2 conditions, including tropical (Houlbrèque et al. 2015) and cold-water corals (Georgian et al. 2016; Büscher et al. 2017; Gómez et al. 2018).

Metabolic rates indicate the energy expenditure of an organism and can be estimated indirectly from oxygen consumption (respiration) rates. In cold-water corals, respiration ranged from significantly increased rates under sudden temperature elevations (Dodds et al. 2007) to significantly depressed rates under elevated pCO_2 (Hennige et al., 2014*a*; Georgian et al. 2016) or elevated temperature (Hennige et al. 2015), to unchanged rates under prolonged acidification (Maier et al. 2013*a*) and/or warming (Hennige et al. 2015). Little has been reported on combined measurement of growth and metabolic activity, although these physiological processes are closely interlinked and may be impacted differently by changing environmental conditions (Hennige et al. 2015).

Dead coral framework is particularly affected by ocean acidification, because in contrast to live corals, dead coral skeletons are not protected by organic tissue and are therefore prone to chemical dissolution in corrosive waters. Together with the onset of bioerosion (including biocorrosion and bioabrasion), this could reduce net reef growth and impair the structural integrity of the reef framework. Bioerosion is thought to contribute more to reef degradation globally than physical erosion or passive chemical dissolution (Schönberg et al. 2017) and, thus, plays an important role in carbonate (re)cycling. In warm-water coral reefs, chemical bioerosion by microphytes and excavating sponges was accelerated significantly under ocean acidification (Tribollet et al. 2006, 2009; Wisshak et al. 2012, 2013), highlighting the need to consider this process in assessments of ocean change impacts (*see* Schönberg et al. 2017 for a review). Bioerosion has been more extensively studied in shallow-water settings, but Beuck and Freiwald (2005) characterized bioerosion patterns of a *L. pertusa* coral mound in the northern Porcupine Seabight in the North Atlantic. Bioerosion was dominated by heterotrophic organisms including bacteria, bryozoans, foraminiferans, fungi, and excavating sponges, the last two groups being the drivers of bioerosion in cold-water coral ecosystems. These bioeroders predominantly colonize tissue-free regions of a coral skeleton, but can expand into the living polyp zone (Beuck and Freiwald 2005). In situ bioerosion rates of dead *Lophelia* framework were recently investigated in a 1-yr deployment and recapture field experiment in cold-water coral reefs off mid-Norway in the North Atlantic (Büscher et al. 2019), giving a first estimate of the contribution of framework bioerosion to net growth in a reef of ~ 16–20% of the production rates by live coral calcification.

Here, we quantify for the first-time responses of both live corals (calcification, respiration, mortality) and dead coral framework (dissolution and bioerosion) of *L. pertusa* simultaneously under ocean acidification and warming; thus considering the balance between coral growth and degradation, which better allows prediction of the fate of cold-water coral reefs under future ocean conditions.

Materials and methods

Sampling and maintenance of *L. pertusa*

L. pertusa samples were collected from an inshore Norwegian cold-water coral habitat in the outer Trondheim-Fjord near Nord-Leksa (63°36.4′N, 09°22.7′E) using the manned submersible JAGO (GEOMAR 2017) during RV POSEIDON

(GEOMAR 2015) cruise POS455 in June/July 2013. Medium-sized branches of white and orange colonies were collected from spatially distinct locations (≥ 50 m distance between colonies) from the reef edges at depths between 150 and 230 m. The corals were placed in large holding tanks on board and cultivated at ambient seabed temperature (7.5°C ± 1°C) until transportation to the laboratory. In the climate-controlled laboratory facility at GEOMAR, corals were kept in a closed recirculating system of 1700 L at near in situ conditions (7.8°C ± 0.2°C temperature and 35.8 ± 0.6 salinity) for half a year. During cultivation in the recirculation system, water was replaced bi-weekly with natural North Sea water enriched in salinity, and corals were fed twice a week with freshly hatched *Artemia franciscana* nauplii (Premium, Sanders).

For the experiment, colonies were fragmented into smaller branches of 38 ± 10 polyps. The experimental fragments were attached to small plastic racks to keep them in an upright position. These racks were equipped with a vinyl (PVC) hook to enable easy handling without touching the animals for the duration of the experiment (Fig. 1). Similar racks were prepared for dead coral framework, but before being attached to the racks, dead framework was examined for the presence of bioeroding organisms by identifying bioerosion trace assemblages according to Beuck et al. (2010). Different bioerosion stages were distributed as evenly as possible to the racks. Similar to the procedure in Büscher et al. (2019), the dead framework was also examined for calcifying epibionts that were carefully removed to eliminate calcification on those fragments. All experimental fragments remained in the recirculating system for another 6 weeks to recover from fragmentation. Afterward, the racks with live corals and dead coral framework were transferred to smaller, independent aquaria of 55 L each (Fig. 1b,c). Fragments were distributed randomly to the experimental aquaria, however, ensuring that fragments from the same colony were not assigned to the same treatment. Each experimental aquarium (= replicate) was equipped with one white, one orange and one dead coral fragment which were acclimatized for 10 d before first measurements took place.

Experimental design and setup

The experiment lasted 13 months and consisted of three treatments which were gradually increased in temperature (T1), pCO_2 level (T2), and both in combination (T3) (Table 1). Each treatment comprised three replicates (three independent aquaria) that were kept under ambient conditions throughout the experiment (control replicates), and seven replicates that were exposed to treatment conditions (manipulated replicates).

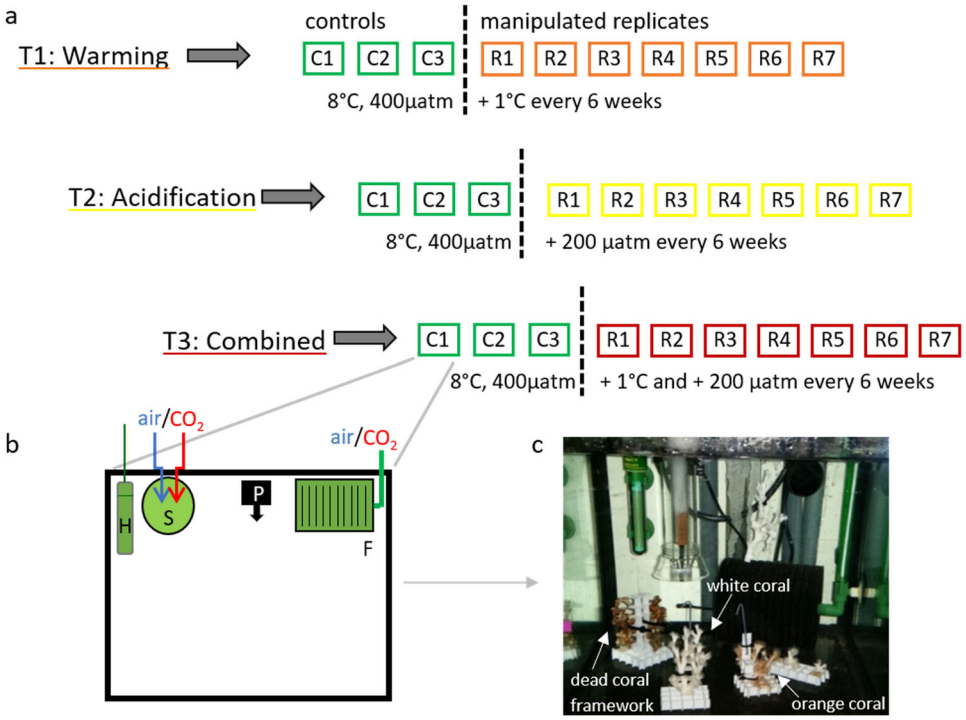

Fig. 1. Schematic visualization of the experimental set-up. (**a**) The three treatments T1 (warming), T2 (acidification), T3 (combined warming and acidification), each containing three controls (C1-3, green boxes) and seven manipulated replicates (R1-7, orange (T1), yellow (T2) and red (T3) boxes). The staggered display of the three treatments shall indicate the time lag of 1 week between the start of the treatment intervals with T2 starting 1 week after T1 and T3 starting 1 week after T2. (**b**) Schematic top view of one experimental aquarium (= replicate) equipped with filter (F), streaming pump (P), skimmer (S), and heater (H). (**c**) Front view of one of the experimental aquaria with sample racks equipped with white, orange, and dead coral fragments.

Table 1. Target temperature (T in°C) and pCO_2 (in μatm) levels of the three treatments T1 (warming), T2 (acidification), and T3 (combined warming and acidification) for each 6-week interval. Note that all replicates in control and manipulated treatment aquaria remained at ambient (= near in situ) conditions for the first two before the onset of temperature and/or pCO_2 elevation.

	T1				T2				T3			
	Control ($n = 3$)		Manipulated ($n = 7$)		Control ($n = 3$)		Manipulated ($n = 7$)		Control ($n = 3$)		Manipulated ($n = 7$)	
Interval	T (°C)	pCO_2 (μatm)	T (°C)	pCO_2 (μatm)	T (°C)	pCO_2 (μatm)	T (°C)	pCO_2 (μatm)	T (°C)	pCO_2 (μatm)	T (°C)	pCO_2 (μatm)
0	8	400	8	400	8	400	8	400	8	400	8	400
1	8	400	8	400	8	400	8	400	8	400	8	400
2	8	400	8	400	8	400	8	400	8	400	8	400
3	8	400	9	400	8	400	8	600	8	400	9	600
4	8	400	10	400	8	400	8	800	8	400	10	800
5	8	400	11	400	8	400	8	1000	8	400	11	1000
6	8	400	12	400	8	400	8	1200	8	400	12	1200
7	8	400	13	400	8	400	8	1400	8	400	13	1400
8	8	400	14	400	8	400	8	1600	8	400	14	1600
9	8	400	15	400	8	400	8	1800	8	400	15	1800

The treatment conditions for the manipulated replicates were elevated by 1°C in temperature (T1), 200 μatm in pCO_2 (T2), or both simultaneously (+1°C and +200 μatm) (T3) every interval (Table 1). One interval covered a 6-week period to give the corals time to acclimatize. The interval periods of the three treatments were initiated consecutively with a time lag of 1 week between T1 and T2, as well as between T2 and T3.

At the end of each interval, calcification and respiration rates of all live corals and bioerosion/dissolution of dead coral fragments were measured. The first measurement week consequently comprised measurements of the three control replicates and the seven manipulated replicates of the temperature treatment (T1), followed by measurements of controls and manipulated replicates of the CO_2 treatment (T2) 1 week later and replicates of the combined treatment (T3) another week later. The adjustment of the next increment in terms of temperature and/or pCO_2 was likewise carried out in succession for the three treatments.

Measurements were taken at the end of each interval, in the last week before adjustments for the next interval manipulation took place. The first three intervals (0–2) comprised measurements under ambient conditions (8°C and ~ 400 μatm) for all replicates of all treatments to determine baseline growth, before first manipulation took place in interval 3 (Table 1). All measurements took place within the experimental aquaria to minimize disturbance.

All 30 aquaria were equipped with a streaming pump (Hydor® KORALIA Nano, flow rate 900 L h^{-1}) for water circulation, a biological air filter (Tropical® Delfin SINGLE), an internal protein skimmer (Aqua Medic® miniflotor 200), a heater (Jäger, 75 W) regulated via a temperature regulator (Hobby® Biotherm Pro), and a pH probe connected to an aquaristic computer (IKS® aquastar) for permanent control of the pH. A CO_2-air-mixture for the CO_2 enriched treatment replicates was provided through KICO2 (Kiel CO_2 manipulation experimental facility; Bleich et al. 2008) and added to every aquarium through an air stone in the skimmer and the filter sponge. Twice a week, pH, temperature, and salinity were measured in every aquarium with a portable pH meter (WTW® pH 3310 equipped with a Sentix-81 pH probe) and conductivity meter (WTW® Cond 3210 with a TetraCon® 325 probe). The salinity was kept constant by regulating evaporation through the addition of distilled water when deviating from 35.2. Feeding was carried out once a week with a homogenous seawater solution (50 mL) containing freshly hatched *A. franciscana* nauplii (> 3 nauplii mL^{-1}) added to every aquarium. Food concentration was adjusted to a medium amount of food based on experiences from a previous long-term study (*see* Büscher et al. 2017). After the start of a new interval, 50% of the water in each aquarium was exchanged by fresh seawater, preadjusted to the respective experimental conditions.

Carbonate chemistry and dissolved inorganic nutrients

Water samples for carbonate chemistry analysis were taken in the same successive mode at the end of each incubation step (every 6 weeks) in the same week that the experimental measurements took place. Duplicate samples of total alkalinity (TA) and dissolved inorganic carbon (DIC) were taken with a 100-mL syringe (Omnific® Solo, BRAUN), sterile filtered (0.2 μm) using a Filtropur L filter (SARSTEDT), and poisoned with $HgCl_2$ using 0.02 vol% saturated solution to arrest biological activity. Samples were stored refrigerated until analysis. TA samples were analyzed via potentiometric open-cell titration (862 Compact Titrosampler, Metrohm). DIC was analyzed

by infrared detection of CO_2 using an Automated Infra-Red Inorganic Carbon Analyzer (AIRICA with *LI-COR 7000*, Marianda). TA and DIC were corrected against Certified Reference Material from A.G. Dickson (Scripps Institution of Oceanography) and density-corrected. Precision of TA duplicates was 4 μmol kg_{sw}^{-1} on average across all samples. The coefficient of variation (given by the AIRICA, which analyses each sample four times) was 1.5 on average. The remaining parameters of the carbonate system: pH (total scale), pCO_2, bicarbonate ions (HCO_3^-), carbonate ions (CO_3^{2-}), and aragonite saturation (Ω_{Ar}) were calculated in Excel® (Microsoft® Office 2019) using the carbonate chemistry macro CO2SYS_v2.1 provided by Pierrot et al. (2006), taking the thermodynamic constants of Mehrbach et al. (1973), refitted by Dickson and Millero (1987).

Samples for analysis of dissolved inorganic nutrients, that is, nitrate + nitrite ($NO_3^-:NO_2^-$), nitrite (NO_2^-), ammonium (NH_4^+), and phosphate (PO_4^{3-}), were sterile filtered as described above and stored refrigerated until analysis on the same day using a four-channel Automated Continuous Segmented Flow Analyzer (A3, SEAL Analytical) according to methods described by Hansen and Koroleff (1999). Detection limits were 0.05 μmol L^{-1} for $NO_3^-:NO_2^-$, 0.06 μg L^{-1} for NO_2^-, 0.04 μmol L^{-1} for NH_4^+, and 0.02 μmol L^{-1} for PO_4^{3-}. Nitrate (NO_3^-) concentrations were calculated by subtracting NO_2^- from the combined $NO_3^-:NO_2^-$ values. The nutrients were analyzed to monitor the water quality (see Supporting Information Fig. S1).

Determination of net calcification and bioerosion/dissolution rates

Net growth (calcification/dissolution) rates of live corals and degradation (net bioerosion/dissolution) rates of dead coral framework were determined using the buoyant weighing technique (Davies 1989). For this, a high precision analytical balance (Sartorius CPA225D, readability = 0.1 mg) was placed on top of the experimental aquaria. Live and dead coral fragments were weighed under water by hanging the coral racks with the hook attached to the below-balance weighing facility using long forceps. Each rack was weighed at least twice to a precision of ± 1 mg buoyant weight. Resulting rates are expressed as weight gain or loss per day as a percentage of the initial weight of the fragment (G in % d^{-1}) similar to descriptions in Büscher et al. (2017). To further improve accuracy of the measurements, the specific density of seawater was calculated with temperature and salinity values recorded in every aquarium at the time of weighing and the specific skeletal density of *L. pertusa* as determined in Büscher et al. (2019) was used for density corrections as described in Davies (1989). Results of live corals were normalized to the specific organic content (ash-free dry mass [AFDM]) of each coral specimen determined at the end of the experiment. The AFDM was gained by drying the specimens to constant weight at 60°C (at least 1 week, depending on individual specimens) before placing them in a muffle furnace at 500°C for 5 h to remove organic residue. Then, specimens were weighed again and the difference in the weight before and after ashing yielded the organic matter. Dead coral framework was standardized to dry weight. All rates were also converted to average surface area of live coral skeletons or bioeroded substrate, respectively (as widely used in bioerosion and carbonate budget analyses). Conversions were performed based on regression analyses from several surface-area/volume/weight correlations of fragments from an earlier experiment (R^2 = 0.988; Büscher et al. 2019).

The observed decline in calcification rates in the control groups under ambient conditions is assumed to be taking place in the manipulated replicates as well in addition to the treatment effects. To estimate the effect size of the treatment impacts without tank/time (= cultivation) effect, the mean calcification rates of all three control groups (T1, T2, T3) were averaged for every interval for white and orange corals. The decline over time revealed by a linear regression analysis (Supporting Information Fig. S2) of all control specimens over all intervals (performed in Excel®) was subtracted from the average calcification value of manipulated corals at each interval. Supporting Information Fig. S3 shows this did not change the overall outcome but emphasizes the potential true effect size of the pCO_2 and temperature manipulations.

Determination of respiration rates (oxygen consumption)

Oxygen consumption rates of all live coral branches were measured using an optode-based oxygen analyzer (Oxy-10 mini, PreSens GmbH). This took place in the 10 aquaria of each treatment simultaneously and was conducted in 800-mL acrylic glass incubation chambers. First, white corals were placed carefully into the chambers, avoiding contact with the coenosarc or exposure to air. Incubation in closed chambers did not exceed 10 h to keep the oxygen concentration within the chambers normoxic (above 70% oxygen concentration; compare Dodds et al. 2007). The same procedure was carried out with the orange corals the following day. The optodes (PreSens oxy-SP-PSt3-NAU-D5-YOP) were calibrated at the beginning of the experiment using a two-point calibration against 0% oxygen concentration established by means of a saturated sodium sulfite (Na_2SO_3) solution, and 100% oxygen saturation via fully aerated seawater. The measurements were logged with the corresponding PreSens software (oxy-10v3_33FB) at an interval of 1 min. Water circulation within the closed chambers was ensured by model making ship's propellers (Graupner) that were powered by 12-V electric motors (Igarashi). The night before every coral respiration measurement, oxygen consumption in the aquarium water was measured to account for sensor drifts. Microbial background respiration was quantified at the end of the experiment in all aquaria in closed chambers filled with ambient seawater from the respective aquaria. Coral respiration rates were derived from the recorded depletion of oxygen over time during the

10-h incubations and corrected for microbial background respiration from the last measurement interval (assuming microbial respiration did not change significantly over time and with the changing treatment conditions). Respiration rates were normalized to AFDM and expressed as μmol O_2 g_{AFDM}^{-1} h^{-1}, accounting for the water volume and the time span of the incubation. Visualizations of the treatment effects corrected for the change in controls similar to calculations for calcification/degradation rates are shown in Supporting Information Fig. S4.

Determination of polyp mortality

Dead polyps were removed from the fragments during fragmentations prior to the experiment. Fragments were examined regularly under water for necrotic or dead polyps and counted during each interval. Mortality was then computed as percentage per coral branch and per conditional increment.

Statistical analysis

Statistical analyses were performed using the statistics graph and data analysis program SigmaPlot© Version 13.0 (Systat Software Inc.) and R version 4.1.2. All data are given as mean ± standard deviation (SD). The raw data are available at Data Publisher for Earth & Environmental Science PANGAEA® under the following url: https://doi.org/10.1594/PANGAEA.947285 (*see* Büscher et al. 2022).

Since the experimental replicates were repeatedly measured over the course of the 13-month experiment, repeated measures ANOVA (RM ANOVA) tests were performed in R to test for changes in physiological responses over time (controls) and with gradual increases in temperature and pCO_2 (manipulated). RM ANOVAs were performed for the dependent variables growth, bioerosion/dissolution, and respiration for both control and manipulated replicates of all treatments (T1: warming, T2: acidification, T3: combined warming and acidification). Carbonate chemistry changes in T2 and T3 were tested similarly to verify that pCO_2 levels were significantly different between intervals.

To figure out where in the experiment significant differences occurred between treatments, treatments (T1, T2, T3) were additionally compared at the individual intervals. For this one-way ANOVA tests (SigmaPlot) were performed (Kruskal–Wallis ANOVA on ranks as nonparametric alternative) for controls and manipulated corals with subsequent post hoc tests (Holm–Sidak method) for pairwise multiple comparison of the different measurement intervals to reveal which treatments differed (Tukey test for nonparametric procedures on ranks). One-way ANOVAs were corrected for enhanced probability of a Type I error using a Bonferroni correction. The new significance level is $p = 0.006$ for both live corals and dead coral framework. Since the control groups did not differ significantly at any of the intervals in any of the tested parameters (growth, respiration, degradation), responses of manipulated corals were then tested against the combined controls ($n = 9$) at each interval to increase statistical power.

Where only two groups were compared (e.g., white and orange average coral performance over the course of the experiment), *t*-tests were applied or a Mann–Whitney rank sum test in case of nonparametric data distribution.

Correlations between calcification and respiration rates were tested by linear regression analysis in SigmaPlot.

Results

Experimental conditions

Target temperature and pCO_2 levels were met throughout the experiment except for the last three to four intervals in the acidification treatments (T2 and T3), where the desired target values of plus 200 μatm were not fully realized at each interval likely caused by a buffering effect resulting from dissolution of the coral skeletons at $\Omega_{Ar} \leq 1$ (Supporting Information Table S2). For more details of the experimental conditions, see Supporting Information.

Calcification rates of live corals

Mean net calcification rates of all live specimens were variable and ranged from −0.0136% to 0.0598% d^{-1} (Table 2). Average calcification rate of nonmanipulated corals (controls) of all treatments and measurements throughout the experiment was 0.0112% ± 0.0098% d^{-1}. Orange corals had significantly higher growth rates (0.0175% ± 0.0104% d^{-1}) than white ones (0.0048% ± 0.0023% d^{-1}) (*t*-test, $p = 0.015$; Supporting Information Fig. S5a). The difference in calcification rates between the colormorphs was particularly evident in the beginning of the experiment, where orange corals increased their calcification rates until the 3rd to 4th interval, after which rates dropped to similar levels as the white specimens in the last (9th) interval (Fig. 2; Supporting Information Fig. S5a). The increase in growth rates in the orange corals during the first few intervals was observed in both controls and manipulated corals (Fig. 2). Orange replicates had also higher variances in calcification rates than white specimens.

There was a time/cultivation effect with consistently declining growth rates throughout the experiment, which was more pronounced in orange corals due to the initial increase in calcification rates (Supporting Information Figs. S2, S5a).

For both colormorphs, treatment-specific responses were similar with warming having an increasing effect on calcification rates and acidification resulting in decreased rates compared to the controls, while combined warming and acidification (T3) appeared to remain similar to the controls (Fig. 2). The decreasing trend of calcification rates as a response to acidification in T2 resulted in lower average calcification in manipulated corals compared with the controls from interval 6 onwards, with dissolution occurring from the 6th interval in white and from the 7th interval in orange corals (Fig. 2).

Table 2. Net calcification/dissolution rates of live corals and net bioerosion/dissolution rates of dead coral framework of the three treatments (T1: warming, T2: acidification, T3: combined warming and acidification) for each 6-week interval of control ($n = 3$) and manipulated ($n = 7$) fragments in weight change in percent per day (% d^{-1}) and computed to coral surface area per year (g m^{-2} yr^{-1}).

		White corals				Orange corals				Dead coral framework			
	Interval	Control (% d^{-1})	Control (g m^{-2} yr^{-1})	Manipulated (% d^{-1})	Manipulated (g m^{-2} yr^{-1})	Control (% d^{-1})	Control (g m^{-2} yr^{-1})	Manipulated (% d^{-1})	Manipulated (g m^{-2} yr^{-1})	Control (% d^{-1})	Control (g m^{-2} yr^{-1})	Manipulated (% d^{-1})	Manipulated (g m^{-2} yr^{-1})
T1	1	0.0099 ± 0.0050	51.2	0.0092 ± 0.0036	47.9	0.0243 ± 0.0091	116.4	0.0433 ± 0.0435	143.6				
	2	0.0055 ± 0.0029	31.2	0.0094 ± 0.0060	49.0	0.0290 ± 0.0096	137.7	0.0598 ± 0.0747	150.5	0.0043 ± 0.0023	27.9	0.0003 ± 0.0020	2.2
	3	0.0059 ± 0.0038	33.2	0.0088 ± 0.0083	46.3	0.0379 ± 0.0191	177.9	0.0546 ± 0.0358	196.9	−0.0027 ± 0.0007	−17.1	−0.0010 ± 0.0007	−5.5
	4	0.0068 ± 0.0023	37.4	0.0099 ± 0.0068	51.1	0.0380 ± 0.0259	178.6	0.0476 ± 0.0164	216.9	−0.0021 ± 0.0009	−13.2	−0.0009 ± 0.0010	−5.5
	5	0.0064 ± 0.0005	35.3	0.0082 ± 0.0053	43.7	0.0281 ± 0.0162	133.6	0.0369 ± 0.0120	170.7	−0.0002 ± 0.0013	−0.4	−0.0009 ± 0.0008	−5.5
	6	0.0042 ± 0.0007	25.3	0.0112 ± 0.0057	57.3	0.0175 ± 0.0090	85.7	0.0316 ± 0.0095	148.4	−0.0018 ± 0.0007	−11.3	−0.0011 ± 0.0011	−6.8
	7	0.0039 ± 0.0015	24.2	0.0102 ± 0.0070	52.7	0.0133 ± 0.0059	66.7	0.0208 ± 0.0063	97.8	−0.0016 ± 0.0014	−10.0	−0.0014 ± 0.0005	−8.7
	8	0.0035 ± 0.0008	22.1	0.0112 ± 0.0086	57.1	0.0102 ± 0.0047	52.4	0.0125 ± 0.0075	54.3	−0.0009 ± 0.0004	−5.5	−0.0009 ± 0.0011	−5.5
	9	0.0026 ± 0.0010	18.0	0.0059 ± 0.0045	33.3	0.0068 ± 0.0032	37.3	−0.0012 ± 0.0055	−4.7	−0.0004 ± 0.0006	−2.3	−0.0009 ± 0.0008	−5.5
T2	1	0.0054 ± 0.0051	30.9	0.0077 ± 0.0063	41.1	0.0198 ± 0.0085	95.9	0.0233 ± 0.0057	111.7				
	2	0.0036 ± 0.0037	22.6	0.0044 ± 0.0028	26.4	0.0213 ± 0.0159	102.8	0.0242 ± 0.0126	116.0	−0.0008 ± 0.0009	−4.9	−0.0003 ± 0.0015	−1.0
	3	0.0044 ± 0.0003	26.3	0.0042 ± 0.0020	25.2	0.0257 ± 0.0089	122.8	0.0256 ± 0.0178	122.3	0.0003 ± 0.0022	2.2	−0.0013 ± 0.0017	−8.1
	4	0.0039 ± 0.0014	24.0	0.0020 ± 0.0036	15.6	0.0172 ± 0.0089	84.4	0.0200 ± 0.0180	96.9	0.0002 ± 0.0013	1.5	−0.0017 ± 0.0010	−10.7
	5	0.0036 ± 0.0016	22.5	0.0033 ± 0.0031	21.3	0.0060 ± 0.0230	33.5	0.0119 ± 0.0082	60.3	−0.0006 ± 0.0009	−3.6	−0.0014 ± 0.0017	−8.7
	6	0.0016 ± 0.0004	13.8	−0.0003 ± 0.0035	5.2	0.0080 ± 0.0075	42.5	0.0031 ± 0.0051	20.4	−0.0014 ± 0.0008	−8.7	−0.0023 ± 0.0007	−14.5
	7	0.0030 ± 0.0003	20.0	−0.0031 ± 0.0050	−7.5	0.0062 ± 0.0054	34.3	−0.0032 ± 0.0064	−7.8	−0.0018 ± 0.0023	−11.3	−0.0055 ± 0.0017	−35.1
	8	0.0018 ± 0.0012	14.4	−0.0023 ± 0.0031	−4.0	0.0059 ± 0.0046	33.2	−0.0050 ± 0.0073	−16.0	−0.0012 ± 0.0015	−7.5	−0.0043 ± 0.0021	−27.4
	9	0.0010 ± 0.0019	10.8	−0.0069 ± 0.0049	−24.7	0.0033 ± 0.0017	21.5	−0.0136 ± 0.0103	−55.2	−0.0003 ± 0.0005	−1.7	−0.0103 ± 0.0036	−65.9
T3	1	0.0085 ± 0.0066	44.8	0.0059 ± 0.0020	32.9	0.0237 ± 0.0104	113.7	0.0198 ± 0.0161	95.9				
	2	0.0071 ± 0.0035	38.5	0.0042 ± 0.0013	25.3	0.0281 ± 0.0114	133.4	0.0208 ± 0.0165	100.5	0.0004 ± 0.0044	2.8	0.0001 ± 0.0011	0.9
	3	0.0066 ± 0.0028	36.2	0.0054 ± 0.0034	31.0	0.0305 ± 0.0105	144.5	0.0253 ± 0.0218	120.9	−0.0006 ± 0.0032	−3.6	−0.0009 ± 0.0007	−5.5
	4	0.0091 ± 0.0037	47.7	0.0073 ± 0.0028	39.5	0.0231 ± 0.0064	111.0	0.0287 ± 0.0246	136.4	−0.0003 ± 0.0016	−1.7	−0.0021 ± 0.0008	−13.2
	5	0.0058 ± 0.0020	32.7	0.0042 ± 0.0016	25.2	0.0159 ± 0.0071	78.2	0.0189 ± 0.0159	91.8	−0.0005 ± 0.0010	−3.0	−0.0025 ± 0.0008	−15.8
	6	0.0052 ± 0.0025	30.1	0.0048 ± 0.0021	28.3	0.0118 ± 0.0047	59.6	0.0130 ± 0.0067	65.1	−0.0004 ± 0.0006	−2.3	−0.0035 ± 0.0010	−21.6
	7	0.0031 ± 0.0020	20.6	0.0058 ± 0.0024	32.8	0.0087 ± 0.0038	45.8	0.0095 ± 0.0086	49.2	−0.0004 ± 0.0006	−2.3	−0.0032 ± 0.0007	−20.3
	8	0.0051 ± 0.0022	29.7	0.0056 ± 0.0022	31.6	0.0075 ± 0.0040	40.3	0.0039 ± 0.0094	24.1	−0.0004 ± 0.0006	−2.3	−0.0039 ± 0.0014	−24.8
	9	0.0030 ± 0.0022	20.1	−0.0013 ± 0.0031	0.6	0.0046 ± 0.0028	27.3	−0.0077 ± 0.0082	−28.4	−0.0001 ± 0.0007	−0.4	−0.0045 ± 0.0013	−28.7

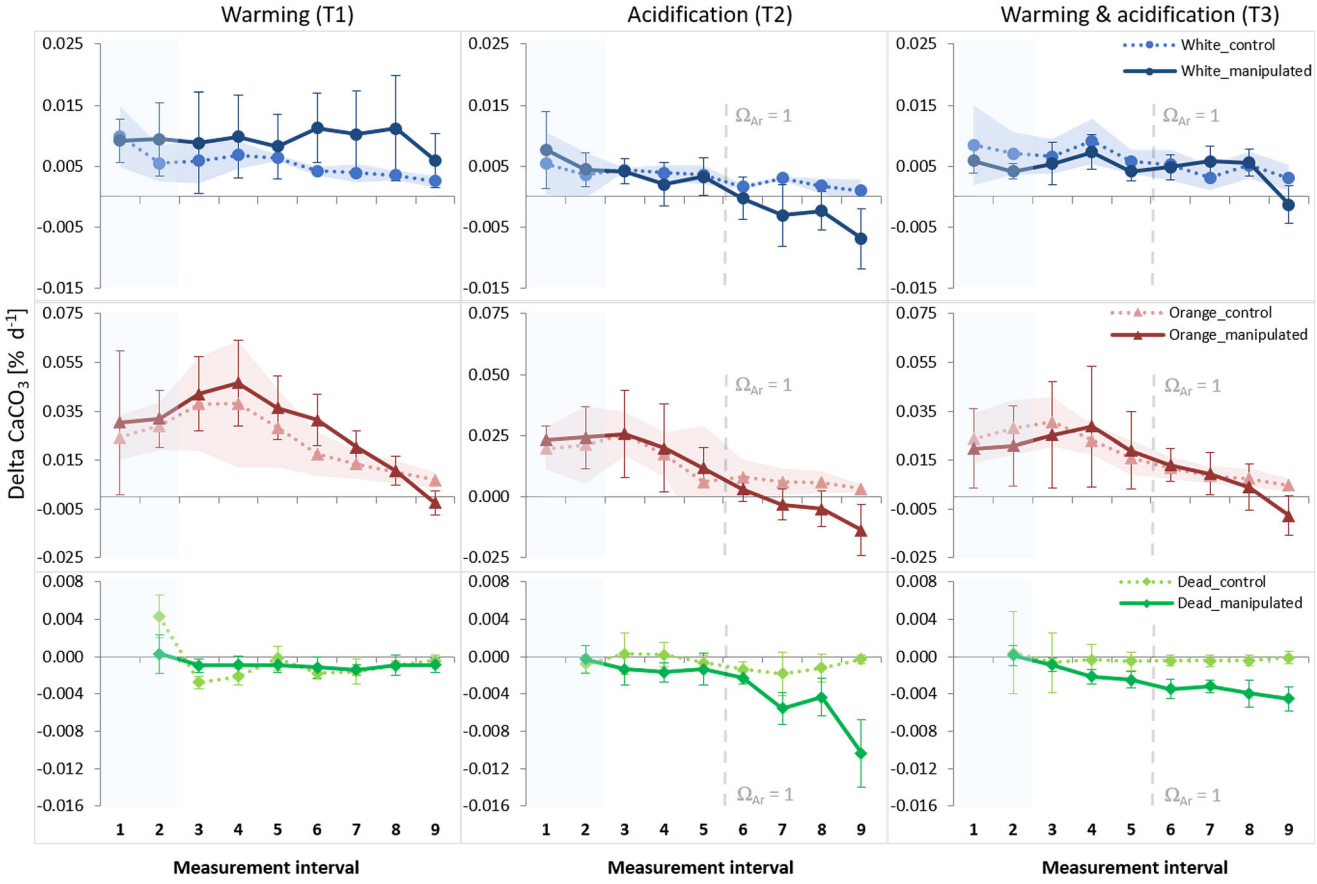

Fig. 2. Growth and bioerosion/dissolution rates (change in mass in % d^{-1}) of controls (light colored, dashed lines, $n = 3$ each) and manipulated specimens (dark colored, solid lines, $n = 7$ each) of white (blue, top row), orange (red, middle row), and dead framework (green, bottom row) fragments of the three treatments T1 (warming, left column), T2 (acidification, middle column), T3 (combined warming and acidification, right column). Depicted are mean values ± SD at every 6-week measurement interval over the course of the 13-month experiment. The standard deviation of the controls is shown as confidence band to improve readability. The shaded area to the left of every graph shows the measurements under ambient conditions before experimental manipulation. Bioerosion/dissolution rate measurements started at interval 1, thus the first rate was yielded at interval 2.

RM ANOVAs revealed statistically highly significant ($p < 0.0001$) differences with regard to the treatment factors and the gradual change over time in both colormorphs.

One-way ANOVAs between treatments revealed that T1 differed significantly from T2 during the last four intervals (intervals 6–9, $p = < 0.001$ to 0.003) in white corals and from intervals 5 to 8 in orange corals ($p = < 0.001$ to 0.004). At interval 6 all treatments differed significantly in orange corals.

Comparing manipulated treatments with a combined control at individual intervals revealed the following distinctions: In T1, a statistically significant difference was only found at interval 6 in white corals ($p = 0.002$) due to high variability in rates (Fig. 2). However, it is noteworthy that during the last interval in T1, calcification rates of manipulated replicates dropped considerably in both colormorphs, resulting in almost 50% decreased calcification in white corals compared to the previous interval and net dissolution of orange corals with 2.5 times as much weight loss (Fig. 2; Table 2).

In T2, manipulated replicates differed significantly from controls in the last four intervals (intervals 6–9, $p = < 0.001$ to 0.004), while in T3 white and orange manipulated replicates did not significantly differ from combined controls, despite a considerable drop in calcification rates that resulted in net dissolution in the last interval (9) in both colormorphs.

While warming slightly elevated growth rates in both colormorphs, it affected them differently with regard to their temperature optima for calcification. Orange corals showed elevated calcification rates at medium elevated temperatures of 9°C to 12/13°C, after which reduction of calcification rates took place, resulting in dissolution at the highest experimental temperature of 15°C. In contrast, white corals increased their calcification rates with increasing temperatures up to 14°C and showed only slightly reduced calcification rates at 15°C and no dissolution. While acidification had a negative effect on calcification rates in both colormorphs leading to increasingly negative calcification with negative net calcification/dissolution at

pCO_2 levels > 1000 μatm ($\Omega_{Ar} \approx 1$) and higher, in the combined treatment, warming and acidification did not show significant effects on growth rates until the last interval. Here, an abrupt breakdown in calcification took place, turning into net dissolution in both colormorphs. While in white corals a slight positive trend was visible at the last two intervals before the breakdown (at 13–14°C and > 1000 μatm), orange corals showed a decreasing trend toward net dissolution already during earlier intervals, similar to the development in both colormorphs in T1.

The effect sizes as a percentage of the manipulated replicates of each treatment corrected for the decline in controls (see Supporting Information Fig. S3) emphasizes these findings and shows that toward the end of the experiment, treatment effects increased in all three treatments.

Respiration (oxygen consumption) rates of live corals

Mean respiration rates ranged from 1.09 to 7.61 μmol O_2 g_{AFDM}^{-1} h^{-1} throughout the experiment with occasional treatment-specific differences (Fig. 3). Coral oxygen consumption was clearly distinct from microbial respiration measured at the end of the experiment (0.11 ± 0.16 μmol O_2 g_{AFDM}^{-1} h^{-1}).

The average respiration rate of all controls was 3.37 ± 1.34 μmol O_2 g_{AFDM}^{-1} h^{-1} over the course of the experiment. Orange controls had 46% higher respiration rates (4.01 ± 1.17 μmol O_2 g_{AFDM}^{-1} h^{-1}) than white controls (2.74 ± 1.20 μmol O_2 g_{AFDM}^{-1} h^{-1}) on average (Supporting Information Fig. S5b), which was highly significant ($p < 0.001$ comparing combined controls of white and orange specimens from the entire experiment, *t*-test). The differences between the colormorphs developed more strongly in a later stage of the experiment. Similar to growth rates, orange specimens showed a higher variation in respiration rates than white specimens (Fig. 3; Supporting Information Fig. S6). Respiration rates decreased over the course of the experiment in corals for most treatments in controls and manipulated corals. This was insignificant between treatments for all controls; however, time had a significant influence on white control corals ($p < 0.001$, RM ANOVA), probably resulting from the stronger increase in respiration rates during the first intervals of the experiment (Fig. 3).

Manipulated replicates showed significant differences with increasing treatment conditions and between treatments in both colormorphs ($p < 0.0001$, RM ANOVA). These include the increase of respiration rates at the beginning of the experiment under ambient conditions, cultivation effect, and treatment effects, but treatment responses were overall comparable to growth responses with a decrease in respiration rates under acidification compared to the controls and an increase in respiration rates under warming (as single stressor or in combination with CO_2) (Fig. 3).

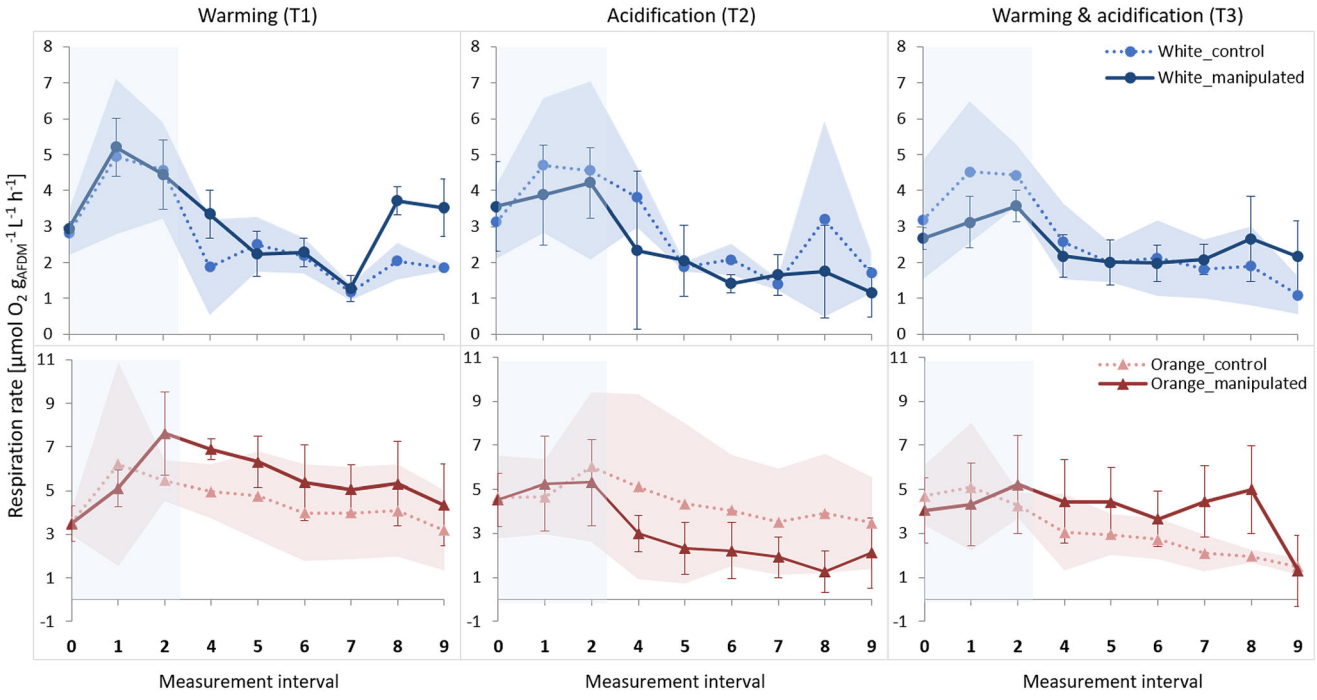

Fig. 3. Respiration (oxygen consumption) rates (in μmol O_2 g_{AFDM}^{-1} h^{-1}) of controls (light colored, dashed lines, $n = 3$ each) and manipulated specimens (dark colored, solid lines, $n = 7$ each) of white (blue, top row) and orange (red, lower row) live corals of the three treatments T1 (warming, left column), T2 (acidification, middle column), T3 (combined warming and acidification, right column). Given are mean values ± SD over the nine measurement intervals of 6 weeks each (*x*-axis). Due to overlapping standard deviation in control and manipulated replicates, the SD of the control replicates is depicted as confidence band. The shaded area to the left of every graph shows the measurements under ambient conditions for all replicates before manipulation started after interval 2.

Comparison of the treatments at individual intervals (one-way ANOVAs) revealed no significant differences between the controls of T1, T2, and T3, but between colormorphs in manipulated treatments. Orange corals were significantly different between treatments from the 4th interval onwards (except intervals 6 and 9) between T1 and T2 and between T2 and T3 in intervals 7 and 8 ($p < 0.001$ in all occasions), whereas white corals showed first significant differences only between T1 and T2 at the very last interval (9; $p < 0.001$).

When comparing respiration rates to the combined controls at individual intervals, only the last interval in T1 (interval 9, $p < 0.001$) and interval 7 in T3 ($p = 0.003$) differ significantly in white corals and intervals 7 and 8 in T2 ($p < 0.001$) in orange corals.

Visualized effect sizes of control-corrected treatment developments clearly demonstrates the increasing trend of respiration rates with warming and decreasing rates with acidification in both colormorphs similar to growth responses (Supporting Information Figs. S4, S3). Both treatment and tank effects became stronger toward the last intervals of the experiment and control-corrected treatment effects were most pronounced in the last two to three intervals. In orange corals, the treatment effects were more pronounced, as respiration rates were continuously elevated throughout the manipulation period in T1 and lowered under acidification in T2, while in white corals, treatment responses were only slightly changing until highest temperatures were reached in T1 and T3 (Supporting Information Fig. S4; Fig. 3).

Respiration was also plotted against calcification (Supporting Information Fig. S6) and showed positive linear relationships in all control corals and in most single stressor treatments, however, in white corals both warming treatments did not or even negatively correlate.

Mortality of live corals

First polyp mortality occurred halfway through the experiment (interval 6). On branches that showed signs of mortality, the number of dead polyps per branch tended to increase with time, especially in manipulated corals. The percentage of dead polyps per fragment at the end of the experiment was generally larger in orange than in white corals, in both control and manipulated replicates (Fig. 4). Between white and orange manipulated replicates in T1 there was a statistically significant difference in the final dead polyp count (Mann–Whitney rank sum test on median values; $p = 0.011$) (Fig. 4).

Polyp mortality was also higher in replicates of all manipulated specimens compared to controls at the end of the experiment, with one exception of an almost entirely dead fragment in the orange controls of T2. This replicate had already lost more than 80% of the polyps when first counted which leads to an increased average mortality percentage in the control group of the pCO_2 treatment (Fig. 4). Eliminating this replicate results in a dead polyp count of the remaining two replicates that is similar to the other control groups (Fig. 4, dashed line). Nevertheless, orange control corals had more than two times higher dead polyp counts than white corals under ambient conditions on average, even when disregarding the nearly dead replicate in T2 controls.

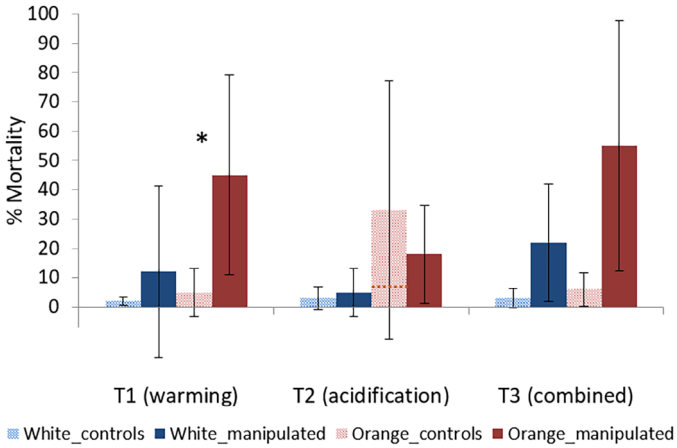

Fig. 4. Mortality as a percentage of dead polyps per fragment of white (blue bars) and orange (reddish bars) corals for control (light colored, dotted bars; $n = 3$) and manipulated (darker colored bars; $n = 7$) replicates of the three treatments T1 (warming), T2 (acidification), T3 (combined warming and acidification) at the end of the experiment (interval 9). Given are mean percentages of the replicates of each group ± SD. The dashed line in the control group of T2 shows the mean percentage of dead polyps in this group when excluding one outlier replicate with > 80% mortality. The asterisk shows a significant difference between white and orange manipulated corals of T1.

Although mortality was consistently low with on average 14% dead polyps per fragment throughout the entire experiment, the amount of dead polyps increased considerably in both warming treatments (unifactorial and combined) toward the end of the experiment with up to 22% (white corals) to 55% (orange corals) average polyp mortality. Highest mortality was observed under combined warming and acidification, followed by warming, while lowest mortality was seen under acidification only. These differences were not significant due to high variability. The control groups were also not significantly different from one another. In the temperature treatments, mortality particularly increased during the last interval of the experiment, between 14°C and 15°C, with manipulated corals showing three times higher mortality on average.

Mortality due to elevated nutrient concentrations can be excluded, as nutrient concentrations remained fairly constant (Supporting Information Fig. S1).

Carbonate degradation of dead coral framework

Net degradation (bioerosion/dissolution) and carbonate accretion rates of all dead coral fragments of the experiment ranged from −0.0103% to 0.0043% d^{-1} (equates to −65.9 to 27.9 g m^{-2} yr^{-1}) (Table 2). Average bioerosion of all three control groups was −0.0006% ± 0.0013% d^{-1} (≈ −3.28 ± 8.35 g m^{-2} yr^{-1}) over the entire experiment duration. There was almost no drift in the controls over time (Fig. 2), thus, in

contrast to the live corals, on dead fragments most likely no tank effect occurred, even though the RM ANOVA points to a time effect in T1 ($p = 0.03$), which is likely caused by the steep drop in the rates from intervals 2 to 3. This initial drop as well as the weight gain in some of the dead fragments during the first one to two intervals in T1 and T2 is probably an artifact arising from trapped air bubbles, which were released during handling in the first weeks of the experiment. The controls did not significantly differ between treatments (RM ANOVA), which is confirmed by one-way ANOVAs at individual intervals, which were all insignificant between treatment controls.

Unlike the controls, manipulated fragments showed significant differences with increasing treatment conditions over time ($p < 0.0001$, RM ANOVA). At interval 6, T1 differed significantly from T3 and at intervals 7 and 9, T1 differed from T2 ($p < 0.001$ for all occasions, one-way ANOVAs). Compared to the combined controls at individual intervals (one-way ANOVAs), manipulated replicates of T2 showed a significant increase in weight loss from interval 7 onwards ($p \leq 0.002$). Combined acidification and warming (T3) caused a significant increase in bioerosion/dissolution rates starting from interval 5 ($p \leq 0.001$ to $p = 0.004$). There was no significant difference between controls and manipulated replicates at any interval under warming alone (T1).

To evaluate whether abiogenic dissolution below $\Omega_{Ar} = 1$ (the saturation level at which the water is undersaturated with respect to aragonite and favorable for calcium carbonate dissolution) enhances the trend of increasing bioerosion rates seen for $\Omega_{Ar} > 1$, we have performed separate linear regressions for $\Omega_{Ar} \geq 1$ and $\Omega_{Ar} < 1$ as visualized in Fig. 5. In both live corals and dead framework, linear regressions of data below $\Omega_{Ar} = 1$ were steeper than regressions with data at $\Omega_{Ar} \geq 1$. This suggests that below $\Omega_{Ar} = 1$, abiogenic aragonite dissolution contributes markedly to the determined rates both for live (Fig. 5a,c) and dead coral framework (Fig. 5b,d). The relative proportion of abiogenic dissolution and bioerosion in dead framework can then roughly be estimated by reading the difference between the two regressions at a given Ω_{Ar} value, that is, at $\Omega_{Ar} = 0.75$ the contribution of the two processes would be approximately 1 : 1 (Fig. 5d). In other words, the triangular

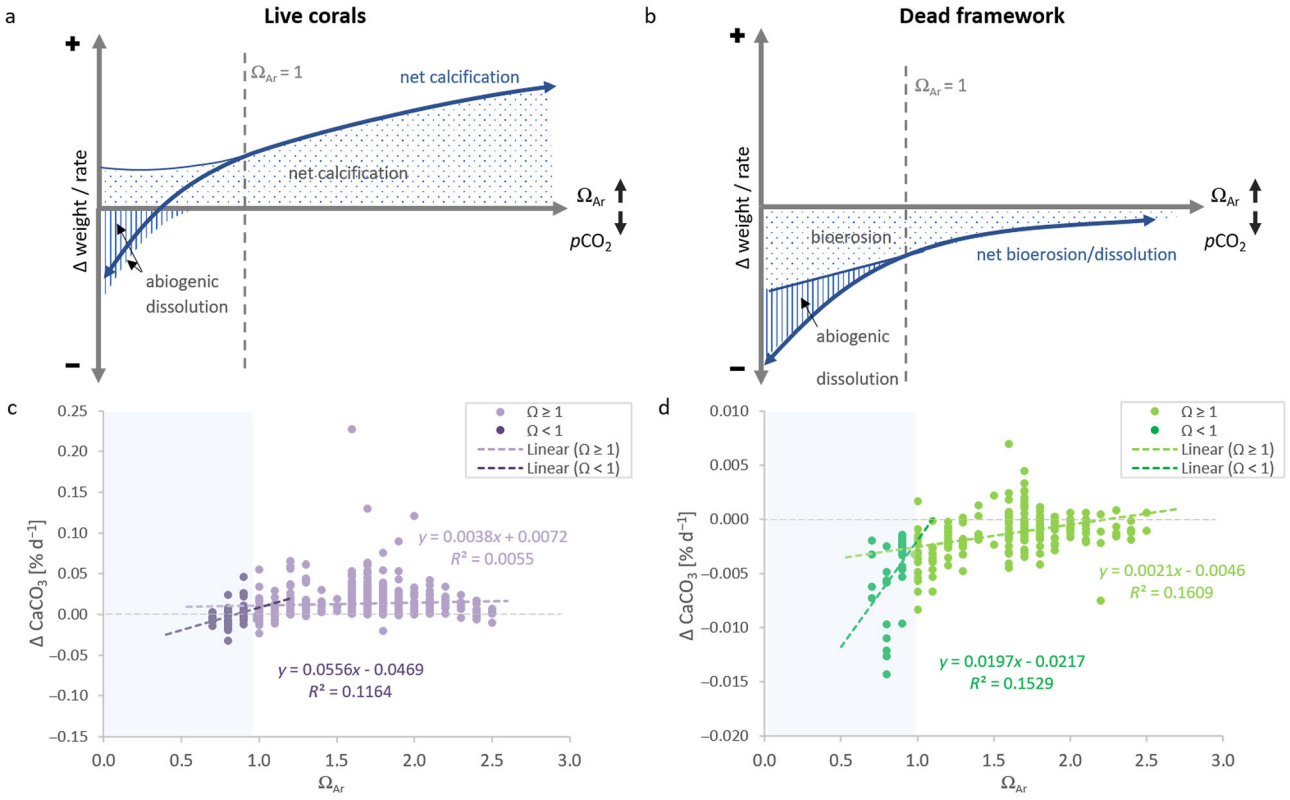

Fig. 5. Net calcification/dissolution rates of live corals (**a**,**c**) and dead coral framework (**b**,**d**) gathered from weight change in % d^{-1}. (**a**, **b**) represent a theoretical concept of where positive net calcification and net dissolution of live corals (**a**) and where bioerosion and abiogenic dissolution in dead coral framework (**b**) would be expected. The graphs below depict the measured data of all live (white and orange) corals of the experiment (**c**) and of dead coral framework (**d**) of all treatments). The two distinct linear regressions are based on values at $\Omega_{Ar} \geq 1$ for and values at $\Omega Ar < 1$ (dark purple for live corals (**c**) and dark green for dead coral framework (**d**)). For aragonite undersaturated waters, the area between the extended linear regressions of $\Omega_{Ar} \geq 1$ and Ω Ar < 1 roughly identifies where abiogenic dissolution increasingly contributes to the measured bioerosion/dissolution rates in dead coral framework (**b**,**d**).

area between the two regressions (in case of dead coral framework), respectively, the steeper regression and the *x*-axis (in live corals) would roughly correspond to abiogenic dissolution.

Discussion

In this study, net growth, respiration and survival, as well as bioerosion/dissolution (biocorrosion/bioabrasion and abiogenic dissolution) of the cold-water coral *L. pertusa* from the North-East Atlantic were examined in a unique study approach under gradual elevation of single or combined ocean change stressors (temperature and pCO_2).

Recent observations of physiological responses to ocean change have shown that combined assessment of multiple stressors differ from unifactorial approaches, including compensation of one another (Büscher et al. 2017; Jiang et al. 2018). It was further highlighted that especially with regard to the slow-growing cold-water corals, short-term exposure responses differ significantly from long-term perturbation responses (Form and Riebesell 2012; Hennige et al. 2015), implying that in the short-term corals show a "shock" response, while after a couple of months they are capable of acclimatizing to altered conditions. While experimental studies on ocean change responses usually look at fixed scenarios of proposed future conditions, our approach used a step-wise gradual increase of CO_2 concentrations and/or temperature to identify physiological optima and potential tipping points. Corals were allowed to acclimatize to increasing stressor levels smoothly through a slow pace of manipulation. In addition, we included for the first-time rates of degradative processes like bioerosion and dissolution of the dead coral framework and its responses to future ocean conditions as opposed to net growth of live corals in simultaneous measurements in our experiment. This is important as the dead portions of cold-water coral assemblages host the majority of associated organisms and may be more strongly affected by dissolution and bioerosion than live corals, but which would weaken the reef framework as a whole and consequently impact biodiversity.

Calcification

Net calcification rates were in accordance with previously reported rates from laboratory experiments and in situ studies at comparable temperatures (Form and Riebesell 2012; Lunden et al. 2014; Kurman et al. 2017).

Although considerable declines in calcification rates were primarily detected after short-term exposure to elevated pCO_2 levels and carbonate undersaturated conditions ($\Omega_{Ar} < 1$), longer-term acidification experiments with *L. pertusa* from different areas including reefs from the Norwegian Sea (Form and Riebesell 2012; Büscher et al. 2017), the Sea of the Hebrides (Hennige et al. 2015), the Gulf of Mexico (Kurman et al. 2017), and the Mediterranean Sea (Maier et al. 2013*b*; Movilla et al. 2014) revealed differential responses ranging from no significant changes in calcification response after 6–12 months of exposure to significant declines. Although some studies emphasize that cold-water corals are able to maintain calcification under moderately elevated pCO_2 conditions, in the majority of those studies a decreasing trend of calcification was observed with increasing pCO_2 levels, with growth rates approaching zero at aragonite undersaturated conditions (Hennige et al. 2015; Büscher et al. 2017). This trend is typically not statistically significant due to high variability among specimens. High variance between replicates demonstrates a high plasticity of this species with regard to environmental conditions (Ragazzola et al. 2013), which is supported by the large bathymetric range and the broad range of environmental conditions inhabited by *L. pertusa*. Kurman et al. (2017) hypothesized that some genotypes may be more resilient to acidification than others, which may explain the generally high variance in responses among specimens in studies with *Lophelia*; however, they found significantly declining net calcification rates over time and net dissolution by the end of the 6-month period in the acidified treatment (pCO_2 = 1160 μatm) of their experiment despite large genotype variances, comparable to our results in the CO_2 treatment (T2, Fig. 2). Experimental studies therefore suggest that *L. pertusa* may reach physiological limits to sustain calcification rates when the water becomes corrosive and/or skeletal dissolution counteracts calcification, eventually leading to lower net growth.

Observations from natural habitats of deep-water corals affirm that some corals can survive low pH (McCulloch et al. 2012*a*; Wall et al. 2015) and at least temporarily even aragonite undersaturated conditions (Davies and Guinotte 2011; Baco et al. 2017). The ability to calcify despite aragonite undersaturation likely results from specialized mechanisms regulating the internal pH level and carbonate ion concentrations at the site of calcification, which "buffers" the pH in the calcifying fluid against external changes of seawater pH (McCulloch et al. 2012*a*,*b*; Wall et al. 2015). However, this ability is species specific, and the process is energetically costly. These energetic costs increase with the increasing gap between external and internal pH under acidification (McCulloch et al. 2012*b*).

Elevated energy demands for pH upregulation as a result of acidification and thermal compensation may eventually result in an energetic imbalance with energy reallocated from other vital processes (Hennige et al. 2015). Jiang et al. (2018) showed that while the negative effects of acidification on calcification of juvenile *P. damicornis* were mitigated by simultaneous warming, the budding process was decelerated under combined temperature and pCO_2 perturbation, which suggests that mitigation comes at a cost to other processes such as reproduction. In the combined treatment of our experiment, the negative effect of elevated pCO_2 as seen in the acidification treatment was partially mitigated by warming, while dissolution occurred only at the highest temperature and CO_2 concentration (14–15°C, 1600 μatm), despite similar aragonite

saturation and pCO_2 conditions as under elevated pCO_2 alone, which may also be attributable to a considerable increase in mortality between 14°C and 15°C. Whether in our experiment calcification was sustained due to efficient upregulation of the internal pH under simultaneous warming and acidification is unclear, but it is very likely that it occurred at the expense of other processes' energy expenditure, especially considering the rapid breakdown at the tolerance threshold in the combined treatment.

Some warm-water scleractinians are able to counteract enhanced energy costs by an increased feeding rate. For some scleractinian species, however, it was observed that food capture rates could not be enhanced to meet additional nutritional demands under acidified conditions, including *L. pertusa* from various spatially distinct populations (Georgian et al. 2016; Büscher et al. 2017; Gómez et al. 2018). The diet of *L. pertusa* consists of a mix of particulate and dissolved suspended organic matter, with zooplankton being the preferentially assimilated food source at Norwegian reefs (Müller et al. 2014; Maier et al. 2019). In the present study, the feeding regime is considered sufficient, as corals appeared to be in good condition visually until the end of the experiment and general experience in cold-water coral husbandry for several years as well as previous experiments under similar feeding conditions have not shown any detrimental signs. However, it cannot be excluded that the cultivation effect seen in this study arose from insufficient nutrition. In a previous long-term experiment, higher vs. lower food availability did not result in altered calcification rates or fitness under ambient or future environmental conditions (Büscher et al. 2017), supporting the incapability of *L. pertusa* to compensate the negative effects of acidification by enhanced feeding.

Respiration

Respiration rates assessed here were in the same range as literature values of *L. pertusa* from the North Atlantic (Larsson et al. 2013; Georgian et al. 2016; Maier et al. 2019) and the Mediterranean Sea (Maier et al. 2013*a*). Metabolic rates of freshly collected corals are generally higher than rates obtained in longer-term laboratory experiments, with rates four times (Dorey et al. 2020) to seven times (Hennige et al., 2014*a*) higher in short-term (on-board) experiments compared to the present and other long-term experiments (Hennige et al. 2015; Georgian et al. 2016). This may either be due to a stress-related increase in respiration after collection (shock response) or due to a reduction in respiration in response to laboratory cultivation (i.e., low-quality food conditions) (Larsson et al. 2013; Hennige et al., 2014*a*). In our experiment, the general decline in respiration rates is most likely attributable to cultivation as this occurred similarly in the controls and in manipulated corals.

Few studies have looked at respiratory metabolism of cold-water corals under ocean acidification and/or warming so far, with contradicting results depending on species, experimental design, duration of exposure, and biogeographic origin of the corals (compare Georgian et al. 2016). Our study lines up with the findings of previous long-term studies (Maier et al. 2013*a*; Hennige et al. 2015), exhibiting no significant changes with respect to acidification or warming compared to control conditions except for a few occasions toward the end of the experiment at highly elevated temperature (white corals) or pCO_2 levels (orange corals). This demonstrates the acclimatization potential of *L. pertusa* to adjust their metabolism under longer-term perturbation of environmental stressors. However, results showed by trend a reduction of respiration rates with acidification and an increase with warming (Fig. 3), similar to calcification responses.

In our experiment, combined increases in temperature and pCO_2 led to elevated respiration rates in *L. pertusa* compared to rates under acidification alone, whereas rates of *Desmophyllum dianthus* were significantly reduced under both stressors, while under single-stressor treatments, respiration tended to increase compared to control conditions (Gori et al. 2016). In contrast, Hennige et al. (2015) measured significantly decreased respiration rates at long-term (12 months) exposure to 3° elevated temperature. Reduced respiration under elevated temperature in combination with a deviation from the usually positively correlating relationship of respiration and calcification was argued to represent a potential shift in energetic pathways, which could be the result of energetic reserves being used by other processes (Hennige et al. 2015). In our case, the relationship between calcification and respiration was only adversely correlated in white manipulated corals in both warming treatments (T1 and T3 in Supporting Information Fig. S6), suggesting that prolonged warming impacts the metabolism of this colormorph in particular. Gori et al. (2016) emphasized a shift from mixed use of proteins, carbohydrates, and lipids as metabolic substrates under control conditions to less efficient protein-dominated catabolism under combined temperature and pCO_2 elevation in *D. dianthus*, which could be an explanation for the imbalance in metabolic and calcification rates in white corals under warming in our experiment as well.

Mortality

In experimental studies with *L. pertusa* from the Gulf of Mexico, where this species usually inhabits waters around 9°C, it was shown that significant mortality occurred at temperatures above 14–15°C (Brooke et al. 2013; Lunden et al. 2014), indicating that this temperature represents a genetically determined upper limit independent of other environmental factors that might influence temperature tolerance. The experimentally identified temperature tolerance limit coincides with the thermal boundary in the biogeographical distribution of this species (Freiwald et al. 2009). In our study, mortality was highest in the combined treatment (Fig. 4), demonstrating the detrimental effects of combined stressors despite or perhaps *because* of the mitigation of physiological

processes under warmer conditions. Interestingly, mortality of orange corals was considerably higher in all treatments (controls and manipulated) compared with white corals, which underpins the observed physiological differences between the two colormorphs.

Differences between colormorphs

L. pertusa and other cold-water corals have distinct color variation arising from carotenoids (i.e., astaxanthin) that occur in the coral tissue and skeleton in higher concentration in orange individuals (Elde et al. 2012). To date, it is unclear whether these astaxanthin variations are genetically or environmentally controlled, but the carotenoids may be derived from the diet (Elde et al. 2012; Osterloff et al. 2019) or transmitted vertically through the eggs of colored colonies (Larsson et al. 2014). The purpose of pigmentation in cold-water corals is not fully resolved yet, but they may serve as antioxidants or as antibacterial agents (Shnit-Orland and Kushmaro 2008; Elde et al. 2012). Colormorphs may also have different nutritional benefits due to specific bacterial compositions (Neulinger et al. 2008).

The fact that genetically distinct individuals of adult white and orange *L. pertusa* skeletally fuse (Hennige et al. 2014*b*) shows that they recognize themselves on the species level and do not reject between individual colonies or different colormorphs in contrast to many tropical coral species, which is a considerable advantage in this framework-forming deep-water coral, as it supports reef stabilization and biodiversity.

An in situ experiment with *L. pertusa* in mid-Norway revealed that growth rates of the orange phenotype are on average twice as high compared to white corals, however, this was again not significant due to the high variability in rates of orange corals, in particular (Büscher et al. 2019). This is in good accordance with the laboratory results of the present study, which showed not only higher physiological rates of orange specimens (up to six times higher calcification rates and 1–2 times higher respiration rates under ambient conditions on average), but also higher standard deviations between replicates (Figs. 2, 3; Supporting Information Fig. S5). The higher variation in rates of orange corals might be related to a higher variation in genotypes between colonies compared with white colonies. Kurman et al. (2017) postulated that a greater genetic variation in genotypes could ensure higher probability of stronger resistance toward ocean acidification. Hence, if orange corals in our study were genetically more diverse than white ones, it could be possible that selective genotypes among the orange corals showed a better performance, which could hold true for Norwegian reefs in general, but this is yet to be verified. Here, we did not find any advantageous responses of the orange phenotype on average with regard to acidification or warming. However, we observed differences in the physiology of both colormorphs with regard to their temperature optima. Although white *L. pertusa* tolerated temperatures up to 15°C fairly well with highest calcification rates at 14°C, optimum temperatures of orange corals for calcification lay in a narrower range between 10°C and 12°C. This would restrict their distribution in the natural environment more than white corals and orange colonies in the Mediterranean Sea, for example, that live already at their tolerance limit would be impacted by increasing temperatures first.

The observed increase in calcification rates in orange corals during the first intervals of the experiment, regardless of treatment attribution, was absent in the responses of white corals. Although fragmentation of white and orange colonies took place at the same time before the experiment, orange corals seem to have acclimatized differently to the same new aquarium environment. Since this observation is evident in all specimens and before manipulation took place, other physiological processes than resulting from the experimental variables must be responsible for this behavior in orange corals. Orange corals also showed a stronger decline in calcification rates toward the end of the experiment than white ones. Both manipulated and control specimens exhibited this pattern, indicating that environmental (cultivation) conditions other than the two manipulated parameters led to less favorable conditions for the orange corals. A potential explanation for this might be that the observed wider range in physiological rates require a higher energy demand, which could not be sustained in the aquarium cultivation in the long term due to a non-sufficient food source. Specimens in our experiment were solely fed with *Artemia* nauplii, which may not provide sufficient carotenoids to sustain a higher concentration of astaxanthin for the orange colormorph to sustain energetic reserves for upregulation of physiological processes and therefore this may have led to a stronger reduction in calcification rates and eventually higher mortality in orange corals. The observation of fading color in orange *L. pertusa* in long-term husbandry of a few years may support this assumption. Beyond that it is noteworthy that orange colonies appear to be more efficient in their physiological performance in a narrower range of environmental conditions than white colonies, which is demonstrated by the faster breakdown and considerable increase in mortality in unsuitable conditions, while white corals withstand similar constraints longer. Altogether, this underlines the important role of seasonally high food availability on Norwegian (fjord) reefs (Maier et al. 2020).

Carbonate degradation of dead coral framework

Carbonate degradation of the dead coral framework by bioerosion and dissolution has received little attention in experimental cold-water coral research so far. Yet, bioerosion represents the natural counterpart of calcification and has become a significant stressor for global reef health and integrity (Schönberg et al. 2017). In cold-water coral bioherms, the dead framework plays an important role as it forms the structural basis of the reefs and hosts the majority of the associated fauna (Freiwald et al. 2004). Accordingly, it has been

emphasized that dissolution and bioerosion of bare skeletons may be the more serious consequences of ocean acidification on cold-water corals than physiological impacts on the live corals (Hennige et al. 2015; 2020).

The prominence of pCO_2 as a factor controlling bioerosion rates is in good accordance to the results of the review and meta-analyses performed by Schönberg et al. (2017) for previous laboratory experiments and field studies on the influence of ocean acidification on different bioeroders worldwide. Although the response of individual bioeroder groups varies strongly depending on ecophysiology and mode of bioerosion, the overall trend indicates an increase in chemical micro- and macro-bioerosion in response to elevated levels of pCO_2, thereby promoting an indirect increase of mechanical bioerosion and grazing (Schönberg et al. 2017). The two principal groups of bioeroders in the aphotic cold-water coral reefs are microfungi and excavating sponges (Beuck and Freiwald 2005; Beuck et al. 2010). To date, there is no experimental data on the influence of pCO_2 on bioerosion rates of microfungi, but bioerosion by phototrophic microborers in tropical coral reefs (chlorophytes and cyanobacteria) significantly increased under simulated ocean acidification (e.g., Tribollet et al. 2006, 2009) and as bioeroding microfungi apply a chemical mode of bioerosion as well, we suspect that fungal microbioerosion is similarly stimulated by elevated levels of pCO_2 as supported by our results. As far as bioeroding sponges are concerned, there is solid experimental evidence for several tropical to cold-temperate species that indicate that they accelerate their bioerosion activity (chemical biocorrosion and mechanical extraction of sediment chips in this case) at elevated pCO_2 levels (Wisshak et al. 2012, 2013; Stubler et al. 2015). This suggests that ecophysiological responses apply across species and latitudes (Wisshak et al. 2014). Since related species of the same sponge genera are abundant in cold-water coral reefs, they are likely affected in the same way. Experiments that have included temperature in separate and combined treatments (Wisshak et al. 2013; Stubler et al. 2015) suggest that temperature has comparatively little effect on the sponge's bioerosion rates until critically high temperature stress levels lead to adverse effects, which is supported by our results.

Selected dead coral fragments showed clear signs of activity of bioeroding microfungi and excavating sponges in our experiment, and while it is safe to assume that grazers were excluded, we cannot separate the contribution by the different agents and types of bioeroders. The settlement of at least the macroborers on the dead framework of *L. pertusa* is patchy, that is, some fragments may have contained bioeroding sponges, while others contained only microborers. The amount and distribution of boring organisms may additionally have been influenced by different biodegradation stages of the dead coral framework (Beuck et al. 2010; Büscher et al. 2019), even though we have made sure to employ advanced stages of bioerosion with presumably mature bioeroder communities only. Besides, we cannot separate bioerosion from abiogenic dissolution, thus, the established rates are to be considered net bioerosion/dissolution rates. However, the first manipulated intervals were in the range of aragonite supersaturation ($\Omega_{Ar} > 1$), so that it can be assumed that abiogenic dissolution came into play only in the last two to four intervals of the T2 and T3 treatments when saturation levels dropped below $\Omega_{Ar} = 1$. Accordingly, separate linear regressions for rates of framework degradation cultivated in saturated vs. undersaturated conditions show that the increase in net bioerosion/dissolution is distinctly more pronounced at $\Omega_{Ar} \leq 1$, an effect interpreted as a result of increasing abiogenic dissolution as depicted in the schematic diagram in Fig. 5.

Our control rates were in the same order of magnitude as bioerosion rates investigated in a 2-yr settlement experiment with pristine limestone tiles carried out at the Säcken *Lophelia* reef in the Swedish Kosterfjord (Wisshak 2006) and with rates from a 1-yr in situ experiment with dead coral framework in comparable biodegradation stages than used in the present experiment in two Norwegian cold-water coral reefs (Büscher et al. 2019). Averaged over the entire course of the experiment, our laboratory rates were slightly lower than the average bioerosion rates of the in situ investigation—a discrepancy that is probably attributable to ecophysiological stress under laboratory conditions and/or a suppressed chance of recolonization compared to an in situ environment.

The accelerated rates of bioerosion/dissolution with elevated pCO_2 suggest that these processes might increasingly compromise the structural integrity of *Lophelia* dominated reef framework and thus pose a potential stress factor for cold-water coral reef health and resilience to ocean change. Together with increased porosity of exposed ("dead") skeleton in live and dead coral framework under acidified conditions as shown by Hennige et al. (2020), the weakening of structural integrity could result in a less complex framework and a breakdown of larger habitats in smaller aggregations of live corals, which was coined as "crumbling" of the reefs by the authors.

Conclusions

L. pertusa is a cold-water coral that shows potential to sustain key physiological processes under ocean acidification and warming. However, in contrast to recent studies which suggest that *L. pertusa* is able to adjust or even adapt to ocean acidification, results of this study show that this species experiences significantly decreasing net calcification rates under prolonged acidification, leading to net dissolution of live corals at aragonite undersaturated conditions, while at the same time, degradation rates (bioerosion and dissolution) of dead coral framework increase with increasing pCO_2, irrespective of temperature, which becomes apparent already at aragonite saturated conditions. This suggests that ocean acidification needs to be considered as a significant promoter of bioerosion and dissolution of cold-water coral reef framework, thus

compromising the structural integrity of these ecosystems under future ocean change. The reef framework as a whole will therefore approach net dissolution sooner than when only live corals are considered.

We compared two commonly co-occurring phenotypes of *L. pertusa* for the first time with regard to their physiological differences and responses to ocean change. Although both colormorphs responded in a similar fashion to warming and acidification, different temperature optima for calcification were observed, which could imply changes in the biogeographical distribution pattern in the future. Although *L. pertusa* is adapted to colder temperatures in the North Atlantic, its optimal temperatures for growth was 10–12°C for orange and 14°C for white corals, which corresponds to 2–6°C higher temperatures than in their natural environment. The increase of calcification rates through warming was impaired by acidification under combined elevated temperature and pCO_2 exposure, but acidification alone was more detrimental than under simultaneous warming. Such compensatory effects likely entail additional energy requirements, which were not met by increased respiration in our experiment and are not likely to be compensated by increased feeding rates, but are probably drawn from other processes such as reproduction to sustain essential functions like calcification.

The combination of decreased calcification rates in live corals and increased degradation of the dead framework makes ocean acidification a serious threat to these valuable ecosystems, which may eventually lead to loss of habitat and biodiversity.

References

Addamo, A. M., A. Vertino, J. Stolarski, R. García-Jiménez, M. Taviani, and A. Machordom. 2016. Merging scleractinian genera: The overwhelming genetic similarity between solitary *Desmophyllum* and colonial *Lophelia*. BMC Evol. Biol. **16**: 108. doi:10.1186/s12862-016-0654-8

Baco, A. R., N. Morgan, E. B. Roark, M. Silva, K. E. F. Shamberger, and K. Miller. 2017. Defying dissolution: Discovery of deep-sea scleractinian coral reefs in the North Pacific. Sci. Rep. **7**: 5436. doi:10.1038/s41598-017-05492-w

Beuck, L., and A. Freiwald. 2005. Bioerosion patterns in a deep-water *Lophelia pertusa* (Scleractinia) thicket (propeller mound, northern porcupine Seabight), p. 915–936. *In* A. Freiwald and J. M. Roberts [eds.], Cold-water corals and ecosystems. Erlangen earth conference series. Springer.

Beuck, L., A. Freiwald, and M. Taviani. 2010. Spatiotemporal bioerosion patterns in deep-water scleractinians from off Santa Maria di Leuca (Apulia, Ionian Sea). Deep-Sea Res. Part II **57**: 458–470. doi:10.1016/j.dsr2.2009.08.019

Bindoff, N. L., and others. 2019. Changing ocean, marine ecosystems, and dependent communities, p. 447–587. *In* H.-O. Pörtner and others [eds.], IPCC special report on the ocean and cryosphere in a changing climate. Cambridge University Press. doi:10.1017/9781009157964.007

Bleich, M., and others. 2008. Kiel CO_2 manipulation experimental facility ($KICO_2$). *In* Second Symposium on the Ocean in a High-CO_2 World. doi:10.13140/2.1.3818.0809

Brooke, S., S. W. Ross, J. M. Bane, H. E. Seim, and C. M. Young. 2013. Temperature tolerance of the deep-sea coral *Lophelia pertusa* from the southeastern United States. Deep Sea Res. Part II **92**: 240–248.

Büscher, J. V., A. U. Form, and U. Riebesell. 2017. Interactive effects of ocean acidification and warming on growth, fitness and survival of the cold-water coral *Lophelia pertusa* under different food availabilities. Front. Mar. Sci. **4**: 101. doi:10.3389/fmars.2017.00101

Büscher, J. V., M. Wisshak, A. U. Form, J. Titschack, K. Nachtigall, and U. Riebesell. 2019. *In situ* growth and bioerosion rates of *Lophelia pertusa* in a Norwegian fjord and open shelf cold-water coral habitat. PeerJ **7**: e7586. doi:10.7717/peerj.7586

Büscher, J. V., A. Form, M. Wisshak, R. Kiko, and U. Riebesell. 2022. Growth, respiration and mortality rates of live *L. pertusa* under gradually amplifying acidification and warming increments and consequences for dissolution and bioerosion of dead coral framework. PANGAEA. doi:10.1594/PANGAEA.947285

Davies, P. S. 1989. Short-term growth measurements of corals using an accurate buoyant weighing technique. Mar. Biol. **101**: 389–395. doi:10.1007/BF00428135

Davies, A. J., and J. M. Guinotte. 2011. Global habitat suitability for framework-forming cold-water corals. PLoS One **6**: e18483. doi:10.1371/journal.pone.0018483

Dickson, A. G., and F. J. Millero. 1987. A comparison of the equilibrium constants for the dissociation of carbonic acid in seawater media. Deep Sea Res. Part A **34**: 1733–1743. doi:10.1016/0198-0149(87)90021-5

Dodds, L. A., J. M. Roberts, A. C. Taylor, and F. Marubini. 2007. Metabolic tolerance of the cold-water coral *Lophelia pertusa* (Scleractinia) to temperature and dissolved oxygen change. J. Exp. Mar. Biol. Ecol. **349**: 205–214. doi:10.1016/j.jembe.2007.05.013

Dorey, N., Ø. Gjelsvik, T. Kutti, and J. V. Büscher. 2020. Broad thermal tolerance in the cold-water coral *Lophelia pertusa* from Arctic and boreal reefs. Front. Physiol. **10**: 1636. doi:10.3389/fphys.2019.01636

Edmunds, P. J. 2011. Zooplanktivory ameliorates the effects of ocean acidification on the reef coral. Limnol. Oceanogr. **56**: 1–11. doi:10.4319/lo.2011.56.6.2402

Elde, A. C., R. Pettersen, P. Bruheim, J. Järnegren, and G. Johnsen. 2012. Pigmentation and spectral absorbance signatures in deep-water corals from the Trondheimsfjord. Norway Mar. Drugs **10**: 1400–1411. doi:10.3390/md10061400

Feely, R. A., C. L. Sabine, K. Lee, W. Berelson, J. Kleypas, V. J. Fabry, and F. J. Millero. 2004. Impact of anthropogenic

CO_2 on the $CaCO_3$ system in the oceans. Science **305**: 362–366. doi:10.1126/science.1097329

Form, A. U., and U. Riebesell. 2012. Acclimation to ocean acidification during longterm CO_2 exposure in the cold-water coral *Lophelia pertusa*. Global Change Biol. **18**: 843–853. doi:10.1111/j.1365-2486.2011.02583.x

Freiwald, A., J. H. Fosså, A. Grehan, T. Koslow, and J. M. Roberts. 2004. Cold-water coral reefs: Out of sight—no longer out of mind, 86 pp. *In* UNEP-WCMC biodiversity series 22. UNEP World Conservation Monitoring Centre.

Freiwald, A., L. Beuck, A. Rüggeberg, M. Taviani, and D. Hebbeln. 2009. The white coral community in the central Mediterranean Sea revealed by ROV surveys. Oceanography **22**: 36–52. doi:10.5670/oceanog.2009.06

GEOMAR Helmholtz-Zentrum für Ozeanforschung. 2015. Research vessel POSEIDON. JLSRF **1**: A36. doi:10.17815/jlsrf-1-62. https://jlsrf.org/index.php/lsf/article/view/62

GEOMAR Helmholtz-Zentrum für Ozeanforschung. 2017. Manned submersible "JAGO". JLSRF **3**: A110. doi:10.17815/jlsrf-3-157

Georgian, S. E., S. Dupont, M. Kurman, A. Butler, S. M. Stromberg, A. I. Larsson, and E. E. Cordes. 2016. Biogeographic variability in the physiological response of the cold-water coral *Lophelia pertusa* to ocean acidification. Mar. Ecol. **37**: 1345–1359. doi:10.1111/maec.12373

Gómez, C. E., L. Wickes, D. Deegan, P. J. Etnoyer, and E. E. Cordes. 2018. Growth and feeding of deep-sea coral *Lophelia pertusa* from the California margin under simulated ocean acidification conditions. PeerJ **6**: e5671. doi:10.7717/peerj.5671

Gori, A., C. Ferrier-Pagès, S. J. Hennige, F. Murray, C. Rottier, L. C. Wicks, and J. M. Roberts. 2016. Physiological response of the cold-water coral *Desmophyllum dianthus* to thermal stress and ocean acidification. PeerJ **4**: e1606. doi:10.7717/peerj.1606

Guinotte, J. M., J. C. Orr, S. D. Cairns, A. Freiwald, L. Morgan, and R. George. 2006. Will human-induced changes in seawater chemistry alter the distribution of deep-sea scleractinian corals? Front. Ecol. Environ. **4**: 141–146.

Hansen, H. P., and F. Koroleff. 1999. Determination of nutrients, p.159–228. *In* K. Grasshoff, K. Kremling, and M. Ehrhardt [eds.], Methods of seawater analysis. Wiley-VCH. doi:10.1002/9783527613984.ch10

Hennige, S. J., L. C. Wicks, N. A. Kamenos, D. C. E. Bakker, H. S. Findlay, C. Dumousseaud, and J. M. Roberts. 2014*a*. Short-term metabolic and growth responses of the cold-water coral *Lophelia pertusa* to ocean acidification. Deep Sea Res. Part II **99**: 27–35. doi:10.1016/j.dsr2.2013.07.005

Hennige, S. J., C. L. Morrison, A. U. Form, J. V. Büscher, N. A. Kamenos, and J. M. Roberts. 2014*b*. Selfrecognition in corals facilitates deep-sea habitat engineering. Sci. Rep. **4**: 6782. doi:10.1038/srep06782

Hennige, S. J., L. C. Wicks, N. A. Kamenos, G. Perna, H. S. Findlay, and J. M. Roberts. 2015. Hidden impacts of ocean acidification to live and dead coral framework. Proc. R. Soc. B **282**: 20150990. doi:10.1098/rspb.2015.0990

Hennige, S. J., and others. 2020. Crumbling reefs and cold-water coral habitat loss in a future ocean: Evidence of "coralporosis" as an indicator of habitat integrity. Front. Mar. Sci. **7**: 668. doi:10.3389/fmars.2020.00668

Henry, L.-A., and J. M. Roberts. 2017. Global biodiversity in cold-water coral reef ecosystems, p. 235–256. *In* S. Rossi, L. Bramanti, A. Gori, and C. Orejas [eds.], Marine animal forests. Springer.

Holocomb, M., D. C. McCorkle, and A. L. Cohen. 2010. Long-term effects of nutrient and CO_2 enrichment on the temperate coral *Astrangia poculata* (Ellis and Solander, 1786). J. Exp. Mar. Biol. Ecol. **386**: 27–33. doi:10.1016/j.jembe.2010.02.007

Houlbrèque, F., S. Reynaud, C. Godinot, F. Oberhänsli, R. Rodolfo-Metalpa, and C. Ferrier-Pagès. 2015. Ocean acidification reduces feeding rates in the scleractinian coral *Stylophora pistillata*. Limnol. Oceanogr. **60**: 89–99. doi:10.1002/lno.10003

Jiang, L., and others. 2018. Increased temperature mitigates the effects of ocean acidification on the calcification of juvenile *Pocillopora damicornis*, but at a cost. Coral Reefs **37**: 71–79. doi:10.1007/s00338-017-1634-1

Kurman, M., C. E. Gómez, S. E. Georgian, J. J. Lunden, and E. E. Cordes. 2017. Intra-specific variation reveals potential for adaptation to ocean acidification in a cold-water coral from the Gulf of Mexico. Front. Mar. Sci. **4**: 111. doi:10.3389/fmars.2017.00111

Larsson, A. I., T. Lundälv, and D. van Oevelen. 2013. Skeletal growth, respiration rate and fatty acid composition in the cold-water coral *Lophelia pertusa* under varying food conditions. Mar. Ecol. Prog. Ser. **483**: 169–184. doi:10.3354/meps10284

Larsson, A. I., J. Järnegren, S. M. Strömberg, M. P. Dahl, T. Lundälv, and S. Brooke. 2014. Embryogenesis and larval biology of the cold-water coral *Lophelia pertusa*. PLoS One **9**: e102222. doi:10.1371/journal.pone.0102222

Lunden, J. J., C. G. McNicholl, C. R. Sears, C. L. Morrison, and E. E. Cordes. 2014. Acute survivorship of the deep-sea coral *Lophelia pertusa* from the Gulf of Mexico under acidification, warming, and deoxygenation. Front. Mar. Sci. **1**: 78. doi:10.3389/fmars.2014.00078

Maier, C., F. Bils, M. G. Weinbauer, P. Watremez, M. A. Peck, and J.-P. Gattuso. 2013*a*. Respiration of Mediterranean cold-water corals is not affected by ocean acidification as projected for the end of the century. Biogeosciences **10**: 5671–5680. doi:10.5194/bg-10-5671-2013

Maier, C., A. Schubert, M. M. B. Sanchez, M. G. Weinbauer, P. Watremez, and J.-P. Gattuso. 2013*b*. End of the century pCO_2 levels do not impact calcification in Mediterranean cold-water corals. PLoS One **8**: e62655. doi:10.1371/journal.pone.0062655

Maier, S. R., T. Kutti, R. J. Bannister, P. van Breugel, P. van Rijswijk, and D. van Oevelen. 2019. Survival under

conditions of variable food availability: Resource utilization and storage in the cold-water coral *Lophelia pertusa*. Limnol. Oceanogr. **64**: 1651–1671. doi:10.1002/lno.11142

Maier, S., R. J. Bannister, D. van Oevelen, and T. Kutti. 2020. Seasonal controls on the diet, metabolic activity, tissue reserves and growth of the cold-water coral *Lophelia pertusa*. Coral Reefs **39**: 1–15. doi:10.1007/s00338-019-01886-6

McCulloch, M., and others. 2012*a*. Resilience of cold-water scleractinian corals to ocean acidification: Boron isotopic systematics of pH and saturation state up-regulation. Geochim. Cosmochim. Acta **87**: 21–34. doi:10.1016/j.gca.2012.03.027

McCulloch, M., J. Falter, J. Trotter, and P. Montagana. 2012*b*. Coral resilience to ocean acidification and global warming through pH up-regulation. Nat. Clim. Change **2**: 623–627. doi:10.1038/nclimate1473

Mehrbach, C., C. H. Culberso, J. E. Hawley, and R. M. Pytkowicx. 1973. Measurement of the apparent dissociation constants of carbonic acid in seawater at atmospheric pressure. Limnol. Oceanogr. **18**: 897–907. doi:10.4319/lo.1973.18.6.0897

Mollica, N. R., W. Guo, A. L. Cohen, K.-F. Huang, G. L. Foster, H. K. Donald, and A. R. Solow. 2018. Ocean acidification affects coral growth by reducing skeletal density. Proc. Natl. Acad. Sci. U.S.A. **115**: 1754–1759. doi:10.1073/pnas.1712806115

Movilla, J., A. Gori, E. Calvo, C. Orejas, À. López-Sanz, C. Domínguez-Carrió, J. Grinyó, and C. Pelejero. 2014. Resistance of two Mediterranean cold-water coral species to low-pH conditions. Water **6**: 59–67. doi:10.3390/w6010059

Müller, C. E., A. I. Larsson, B. Veuger, J. J. Middelburg, and D. van Oevelen. 2014. Opportunistic feeding on various organic food sources by the cold-water coral *Lophelia pertusa*. Biogeosciences **11**: 123–133. doi:10.5194/bg-11-123-2014

Neulinger, S. C., J. Järnegren, M. Ludvigsen, K. Lochte, and W.-C. Dullo. 2008. Phenotype-specific bacterial communities in the cold-water coral *Lophelia pertusa* (Scleractinia) and their implications for the coral's nutrition, health, and distribution. Appl. Environ. Microbiol. **74**: 7272–7285. doi:10.1128/AEM.01777-08

Orr, J. C., and others. 2005. Anthropogenic ocean acidification over the twenty-first century and its impact on calcifying organisms. Nature **437**: 681–686. doi:10.1038/nature04095

Osterloff, J., I. Nilssen, J. Järnegren, T. V. Engeland, P. Buhl-Mortensen, and T. W. Nattkemper. 2019. Computer vision enables short- and long-term analysis of *Lophelia pertusa* polyp behaviour and colour from an underwater observatory. Sci. Rep. **9**: 6578. doi:10.1038/s41598-019-41275-1

Pierrot, D., E. Lewis, and D. W. R. Wallace. 2006. MS Excel program developed for CO_2 system calculations. ORNL/CDIAC-105a. Carbon Dioxide Information Analysis Centre, Oak Ridge National Laboratory, U.S. Department of Energy.

Ragazzola, F., L. C. Foster, A. U. Form, J. V. Büscher, T. H. Hansteen, and J. Fietzke. 2013. Phenotypic plasticity of coralline algae in a high CO_2 world. Ecol. Evol. **3**: 3436–3446. doi:10.1002/ece3.723

Roberts, J. M., and S. D. Cairns. 2014. Cold-water corals in a changing ocean. Curr. Opin. Environ. Sustain. **7**: 118–126. doi:10.1016/j.cosust.2014.01.004

Schönberg, C. H. L., J. K. H. Fang, M. Carreiro-Silva, A. Tribollet, and M. Wisshak. 2017. Bioerosion: The other ocean acidification problem. ICES J. Mar. Sci. **74**: 895–925. doi:10.1093/icesjms/fsw254

Shnit-Orland, M. and A. Kushmaro. 2008. Coral mucus bacteria as a source for antibacterial activity. Proceedings of the 11th International Coral Reef ymposium, Ft. Lauderdale, FL, 7–11 July 2008.

Siegenthaler, U., E. Monnin, K. Kawamura, R. Spahni, J. Schwander, B. Stauffer, T. F. Stocker, J. Barnola, and H. Fischer. 2005. Supporting evidence from the EPICA Dronning Maud Land ice core for atmospheric CO_2 changes during the past millennium. Tellus B **57**: 51–57. doi:10.3402/tellusb.v57i1.16774

Stubler, A. D., B. T. Furman, and B. J. Peterson. 2015. Sponge erosion under acidification and warming scenarios: Differential impacts on living and dead coral. Global Change Biol. **21**: 4006–4020. doi:10.1111/gcb.13002

Tanhua, T., A. Körtzinger, K. Friis, D. W. Waugh, and D. W. R. Wallace. 2007. An estimate of anthropogenic CO_2 inventory from decadal changes in oceanic carbon content. Proc. Natl. Acad. Sci. USA **104**: 3037–3042. doi:10.1073/pnas.0606574104

Tribollet, A., M. J. Atkinson, and C. Langdon. 2006. Effects of elevated pCO_2 on epilithic and endolithic metabolism of reef carbonates. Global Change Biol. **12**: 2200–2208. doi:10.1111/j.1365-2486.2006.01249.x

Tribollet, A., C. Godinot, M. Atkinson, and C. Langdon. 2009. Effects of elevated pCO_2 on dissolution of coral carbonates by microbial euendoliths. Global Biogeochem. Cycl. **23**: 1–7. doi:10.1029/2008GB003286

Vad, J., C. Orejas, J. Moreno-Navas, H. S. Findlay, and J. M. Roberts. 2017. Assessing the living and dead proportions of cold-water coral colonies: Implications for deep-water marine protected area monitoring in a changing ocean. PeerJ **5**: e3705. doi:10.7717/peerj.3705

Wall, M., F. Ragazzola, L. C. Foster, A. Form, and D. N. Schmidt. 2015. pH up-regulation as a potential mechanism for the cold-water coral *Lophelia pertusa* to sustain growth in aragonite undersaturated conditions. Biogeosciences **12**: 6869–6880. doi:10.5194/bg-12-6869-2015

Wisshak, M. 2006. High-latitude bioerosion: The Kosterfjord experiment (Lecture notes in earth sciences), v. **109**. Springer, 202 pp.

Wisshak, M., C. H. L. Schönberg, A. Form, and A. Freiwald. 2012. Ocean acidification accelerates reef bioerosion. PLoS One **7**: e45124. doi:10.1371/journal.pone.0045124

Wisshak, M., C. H. L. Schönberg, A. Form, and A. Freiwald. 2013. Effects of ocean acidification and global warming on reef bioerosion—Lessons from a clionaid sponge. Aquat. Biol. **19**: 111–127. doi:10.3354/ab00527

Wisshak, M., C. H. L. Schönberg, A. Form, and A. Freiwald. 2014. Sponge bioerosion accelerated by ocean acidification across species and latitudes? Helgol. Mar. Res. **68**: 253–262. doi:10.1007/s10152-014-0385-4

Zheng, M.-D., and L. Cao. 2015. Simulation of global ocean acidification and chemical habitats of shallow- and cold-water coral reefs. Adv. Clim. Chang. Res. **5**: 189–196. doi: 10.1016/j.accre.2015.05.002

Acknowledgments

This study was carried out as part of the BMBF (Federal Ministry of Education and Research) funded project BIOACID II (Grant number: FKZ 03F0655A). Coral sampling took place at the outer Norwegian Trondheimsfjord and was conducted with kind permission of the Norwegian Directorate of Fisheries (Fiskeridirektoratet). Rainer Kiko would furthermore like to acknowledge funding via the SFB 754 "Climate-Biogeochemistry Interactions in the Tropical Ocean" (grant number: 27542298 of the German Science Foundation DFG) and via a "Make Our Planet Great Again" grant of the French National Research Agency within the "Programme d'Investissements d'Avenir" (reference: ANR-19-MPGA-0012). The captain and crew of RV POSEIDON are greatly thanked for support during the research cruise POS455. Export and import permits for the cold-water coral *L. pertusa* were obtained through the Convention on International Trade in Endangered Species of Wild Fauna and Flora (CITES) by the Norwegian Environment Agency (Miljø Direktoratet) and the Federal Agency for Nature Conversation (BfN). The authors would like to thank the student assistants Nils Kreuter and Marie Küter for support throughout the experiment, Dr. Lydia Beuck for assistance with coral framework preparations, and Kerstin Nachtigall, Andrea Ludwig, and Jana Meyer for assistance with chemical analyses. Dr. Sandra Brooke and Dr. Rachel Cave greatly thanked for constructive feedback on the manuscript. Dr. Mark Lenz is further greatly thanked for statistical advice. This paper was completed at NUI Galway, Ireland where the lead author has been working on the Ocean Acidification and Biogeochemistry: Variability, trends and Vulnerability (VOCAB) project since April 2020, funded by the Marine Institute of Ireland. The authors would like to extend our gratitude to two anonymous reviewers for their constructive and careful comments. Open Access funding enabled and organized by Projekt DEAL.

Conflict of Interest

None declared.

Submitted 30 April 2021
Revised 08 March 2022
Accepted 09 July 2022

Associate editor: David Michael Baker